J. Fluid Mech. (1993), *vol.* 251, *pp.* 355–375

The hydraulics of a stratified fluid flowing through a contraction

By LAURENCE ARMI AND RICHARD WILLIAMS
Scripps Institution of Oceanography, University of California at San Diego, La Jolla, CA 92093-0230, USA

(Received 22 February 1991 and in revised form 11 December 1992)

The steady hydraulics of a continuously stratified fluid flowing from a stagnant reservoir through a horizontal contraction was studied experimentally and theoretically. As the channel narrows, the flow accelerates through a succession of virtual controls, at each of which the flow passes from subcritical to supercritical with respect to a particular wave mode. When the narrowest section acts as a control, the flow is asymmetric about the narrowest section, supercritical in the divergent section and self-similar throughout the channel. With increased flow rate a new enclosed self-similar solution was found with level isopycnals and velocity uniform with depth. This flow is only symmetric in the immediate neighbourhood of the narrowest section, and in the divergent section remains supercritical with respect to higher internal modes, has separation isopycnals and splits into one or more jets separated by regions of stagnant, constant-density fluid. Flows which are subcritical with respect to lowest modes can also be asymmetric about the narrowest section for higher internal modes. The experiments are interpreted using steady, inviscid hydraulic theory. Solutions require separation isopycnals and regions of stationary, constant-density fluid in the divergent section.

1. Introduction

The flow of a continuously stratified fluid from a stagnant reservoir through a horizontally convergent–divergent contraction is studied here. Geophysical applications include the flow of the stratified atmosphere through mountain gaps, and similar oceanic flows through gaps in mid-ocean ridges or between islands. Even a mesoscale eddy field with a convergent–divergent flow region will induce the flow regime studied here. An engineering application is in the withdrawal of fluid from a stratified reservoir. As a fluid mechanics problem involving hydraulic controls, it is particularly interesting because transitions from subcritical to supercritical flow occur through an infinite set of controls as the flow is accelerated from rest in the reservoir. This is because unlike a single-layer open channel flow or the compressible analogue of flow through a convergent–divergent nozzle, we are dealing with a flow that has essentially an infinite number of characteristics wave speeds, each associated with a wave of different vertical structure. Even a compound-compressible nozzle flow with several streams of gas flowing side-by-side (cf. Bernstein, Heiser & Hevenor 1967) has only one effective characteristic speed.

There is a large body of literature on the flow of a continuously stratified fluid over a sill or mountain ridge. Hydraulic solutions for such flows have been discussed by Long (1955), Smith (1985) and others, and the multi-layer approximation to continuously stratified hydraulics has recently been studied by Baines & Guest (1988).

While the related problem of the flow of a stratified fluid through a horizontal contraction is relevant in a similar variety of engineering and geophysical applications, it has received far less attention. Recent study of the hydraulics of two-layer systems by Armi (1986) shows that in stratified systems, flow over a sill and through a contraction have a fundamentally different character due to the possibility of critical flow at points other than the channel's geometric constriction, a condition first found by Wood (1968) and called a virtual control. Wood also showed that there is a self-similar flow that accelerates from a stagnant reservoir and is controlled at the narrowest point in the channel and through a succession of virtual controls, at each of which the flow passes from subcritical to supercritical with respect to a particular wave mode. This solution was studied further by Benjamin (1981) who showed the hydraulically controlled nature of the flow and conjectured that it is the only solution that can come from a stagnant reservoir. We find a much greater variety of flows than can be explained by the work of Wood or Benjamin.

We will show here that an attempt to decelerate a self-similar flow through a virtual control in the divergent section of the channel results in a flow that remains supercritical and is characterized by separation isopycnals and acceleration of portions of the flow. A search for flows of this type was motivated by the earlier work of Armi (1986) for the two-layer system, where it was seen that although transition through, in this case, a single virtual control in the convergent section resulted in a uniform flow from the reservoir, an attempt to pass back through the same virtual control in the divergent section always resulted in following an intersecting solution branch which accelerated one of the layers and kept the flow supercritical.

In §2, self-similar flows are reviewed. Wood's *internal self-similar flow* is demonstrated, for which fluid is only withdrawn from a limited range of isopycnals and the flow has a strongly depth-dependent velocity profile. The range of densities withdrawn from the reservoir is controlled at the narrowest section. We also demonstrate a new *enclosed self-similar flow* that occurs at higher flow rates, when fluid of all densities is withdrawn from the reservoir and the flow is not controlled at the narrowest section. When the Boussinesq approximation is made, this enclosed self-similar flow is uniform in depth and accelerates uniformly as it enters the contraction. Solutions for these self-similar flows are presented and the equations to be used later in the paper discussed. In §3 flows with separation isopycnals, bifurcating from the enclosed self-similar flow, are shown to form. The separation isopycnals force the existence of one or more layers of stagnant constant-density fluid and one or more high-speed regions in the divergent section of the channel, where the flows are supercritical. In §4, we force an internal self-similar flow to be subcritical at the narrowest section. In the divergent section of the channel we find a bifurcation of the internal self-similar flow, analogous to that found for enclosed self-similar flows, to a flow with separation isopycnals and complex vertical structure that allows the flow to match the downstream conditions.

Throughout the paper, we will see a variety of vertical structures in the fully nonlinear flows that were studied. These nonlinear vertical structures are visually somewhat analogous to the shapes of linear internal wave modes. A velocity profile that is vertically uniform will be referred to as *structure 0*. A profile with a single velocity maximum at the top or bottom of the channel will be referred to as *structure 1*. A profile with a single maximum in the centre of the channel or two maxima, one at each vertical boundary, will be referred to as *structure 2*. More complex profiles follow this convention.

1.1. *Description of the experiments*

Figure 1 (plate 1) is an overview of the experimental facility. A narrow, flat-bottomed Plexiglas channel, 10.2 cm wide, was connected to a $123 \times 246 \times 24$ cm Plexiglas reservoir. Flow into the channel entrance was accelerated slowly by a curved vertical wall leading into the channel. The channel was 2 cm wide at the narrowest section of the contraction. The convergent/divergent section was 86 cm long, so the change in width took place quite gradually. Preliminary experiments with a symmetrical contraction geometry showed that there was a tendency for the flow to separate from one or both walls in the divergent section of the channel. In the channel used here, away from the narrowest section, the divergent section of the channel changed width at half the rate of the convergent section.

Figure 2(*a*) (plate 1) shows the contraction and the downstream section of the channel, and a top view, drawn to scale, is shown in figure 2(*b*). The flow here and in all figures is from right to left. A vertical ruler marks the narrowest point in the contraction. In figure 2(*a*), fluid is being withdrawn from two line sinks, the heights of which were adjustable. A thin slit at the base of the channel endplate, not in use in this photograph but used in figure 3(*a*), allowed fluid to be withdrawn from the base of the channel. Precision gear pumps were used to establish known withdrawal flow rates.

In all experiments, the reservoir was initially filled to a depth of 20 cm. The total flow rate relative to the volume of the reservoir was always such that the free surface descended very slowly and the resulting flow was a good approximation of a steady flow from an infinite reservoir. The reservoir was filled with a salt solution from a double-bucket setup that results in a linear density stratification. The density variation was typically $\sim 0.4\%$ over the depth of the reservoir. While filling the reservoir, the fluid was dyed at various levels with red food colouring. The resulting set of horizontal dye lines were used to visualize the vertical displacement of the density surfaces. A qualitative indication of the velocity field was obtained from vertical dye lines produced by dropping crystals of potassium permanganate into the channel. Both the displacement of the density surfaces and the vertical dye lines can be seen in figure 2(*a*). This flow, which will be discussed in more detail in §4, has a structure-2 profile in the convergent section of the channel on the right-hand side of the figure that splits into a structure-4 profile in the divergent section of the channel. Quantitative measurements of the velocity field were obtained from particle streak photographs (cf. figure 3*b*). Suspended metallic paint pigment was illuminated with a thin vertical sheet of light to avoid sampling particles in the side-wall boundary layers. Data from several nearly simultaneous streak photographs were combined to produce densely sampled velocity profiles at various positions along the channel (cf. figure 5).

2. Self-similar flows

2.1. *Internal self-similar flows*

The first experiment shown in this section duplicates that of Wood (1968); it also extends his work to give a quantitative measurement of the velocity field. When the withdrawal slit is at the channel floor and the flow rate is low, a version of Wood's self-similar solution develops in which all isopycnals from the channel floor up to a separation isopycnal flow through the contraction. We call this an internal self-similar flow and a flow of this type is shown in figure 3(*a*) (plate 2). A streak photograph of a portion of this flow is shown in figure 3(*b*) (plate 2). The vertical dye lines show that the flow is most rapid at the bottom of the channel and decays smoothly with height

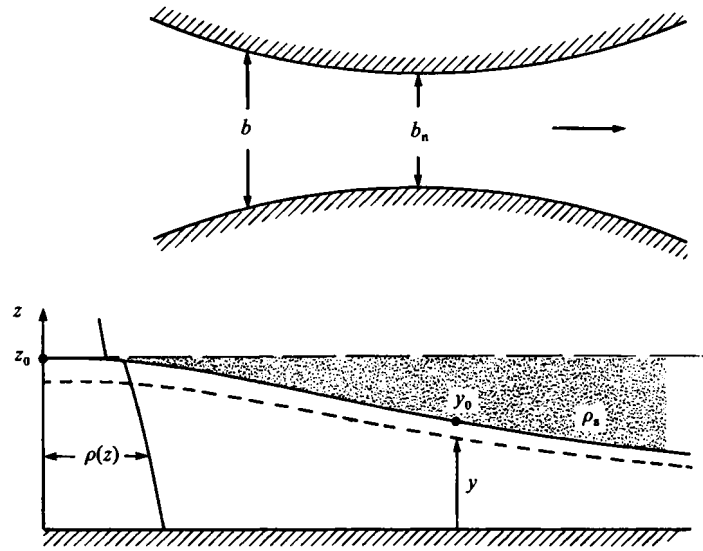

FIGURE 4. Stratified fluid flowing through a horizontal contraction.

up to a separation isopycnal, above which the fluid is motionless; this is a structure-1 velocity profile. Notice that as the moving region thins, there is a region of almost constant density, nearly motionless fluid above the rapidly moving fluid.

At the reservoir, where the fluid is stationary, the flow is subcritical with respect to all internal modes. As the flow accelerates into the contraction, it passes through an infinite sequence of virtual controls. At each successive virtual control, the flow changes from subcritical to supercritical with respect to the next lowest internal wave mode. The flow is asymmetric about the narrowest section, where it is critical with respect to the lowest internal wave mode. The critical point at the narrowest section controls the total range of isopycnals drawn through the contraction. When the total flow rate is increased, fluid is withdrawn from a larger range of isopycnals but the structure of the flow is not altered. In theory, this behaviour can continue until, at the reservoir, the separation isopycnal reaches the free surface. In practice, the presence of a surface boundary layer alters the structure of the solution slightly before this point is reached.

2.2. *Self-similar solutions*

Our development of the equations of motion follows that of Benjamin (1981). The problem to be studied is illustrated in figure 4. The channel has a rectangular cross-section and a horizontal floor, and its breadth b is assumed to vary slowly in the streamwise direction to a minimum b_n at the narrowest section. The subscript n will be used throughout to denote the value of a variable at the narrowest section. The fluid is assumed to be inviscid, incompressible and non-diffusive, and to be flowing steadily with uniform cross-stream velocity. The density of the fluid on any stream surface is constant but varies across these surfaces. The height of a stream surface at the upstream reservoir is taken to be z, and at any downstream location, the height of this surface is written as $y(z)$. The density of the fluid on that surface is $\rho(z)$. The total depth of the moving fluid is z_0 at the reservoir and $y_0 = y(z_0)$ at some downstream location. The fluid above this level is stationary and there may be a density step between the moving fluid and this stagnant region. At the reservoir, the fluid immediately above the moving region has a density ρ_s. In the following development, the stream surface height

y will be taken to be the dependent variable, while the density profile and flow rate per unit depth at the reservoir are assumed to be known functions of z.

The pressure in the fluid is hydrostatic and if $z = z_0$ is taken as a reference level, the pressure in the reservoir below this level is given by

$$p(z) = g\int_z^{z_0} \rho \, d\hat{z}. \tag{1}$$

At any downstream location, the motionless fluid between y_0 and z_0 must be stably stratified with densities between $\rho(z_0)$ and ρ_s. In the case of smoothly varying stratification, the flow may either be confined to less than the full depth of the channel, in which case $\rho_s = \rho(z_0)$, or fluid at all levels may be flowing, in which case the moving fluid is bounded above by a free surface. Both cases can be considered by taking the fluid between y_0 and z_0 to be of constant density ρ_s. The pressure at any level below y_0 is then given by

$$p(y) = g\left(\rho_s(z_0 - y_0) + \int_y^{y_0} \rho \, d\hat{y}\right). \tag{2}$$

The flow on each stream surface is governed by Bernoulli's equation and so

$$\tfrac{1}{2}\rho u^2 + \rho g y + p(y) = H(z) \tag{3}$$

is constant on each stream surface. $H(z)$ is evaluated at the motionless reservoir, where $H(z) = \rho g z + p(z)$. This is substituted into (3), along with (1) and (2), and an integration by parts is performed on each integral, to give

$$\rho u^2 = 2g\left[\Delta\rho(z_0 - y_0) - \int_z^{z_0} (\hat{z} - y)\rho' \, d\hat{z}\right], \tag{4}$$

where $\Delta\rho = \rho(z_0) - \rho_s$ and ρ' denotes $d\rho/dz$. Primes will be used throughout to denote z-derivatives.

Continuity along the channel is expressed by requiring the volume flux in each stream surface to be constant. Thus the volume flux per unit depth is a function of z alone and at some downstream location the flux in a layer of thickness dy must equal the flux at the reservoir in a layer of thickness dz. If $q(z)$ is the volume flux per unit depth, and u and b are the velocity and channel breadth at some downstream location, the $q(z)\,dz = ub\,dy$, or

$$uby' = q(z). \tag{5}$$

Bernoulli's equation (4) and the continuity requirement (5) are combined to give

$$\frac{\rho q^2}{g b_n^2} = 2\frac{b^2}{b_n^2} y'^2 \left[\Delta\rho(z_0 - y_0) - \int_z^{z_0} (\hat{z} - y)\rho' \, d\hat{z}\right]. \tag{6}$$

The left-hand side of (6) is a function of the upstream reservoir conditions alone, so we define

$$f(z) = \rho q^2 / g b_n^2. \tag{7}$$

The problem is now expressed as a second-order differential equation and a pair of boundary conditions by dividing (6) by y'^2 and differentiating with respect to z:

$$(f/y'^2)' + 2\lambda(y - z)\rho' = 0. \tag{8a}$$

Notice that the channel width enters the problem through the parameter $\lambda = b^2/b_n^2$. The boundary conditions are

$$\left.\begin{aligned} &y = 0 \quad \text{at} \quad z = 0; \\ &\text{if} \quad \Delta\rho \neq 0, \quad 2\lambda\Delta\rho(z - y)\,y'^2 = f(z_0) \quad \text{at} \quad z = z_0, \\ &\text{or if} \quad \Delta\rho = 0, \quad y'(z) \quad \text{is regular as} \quad z \to z_0. \end{aligned}\right\} \tag{8b}$$

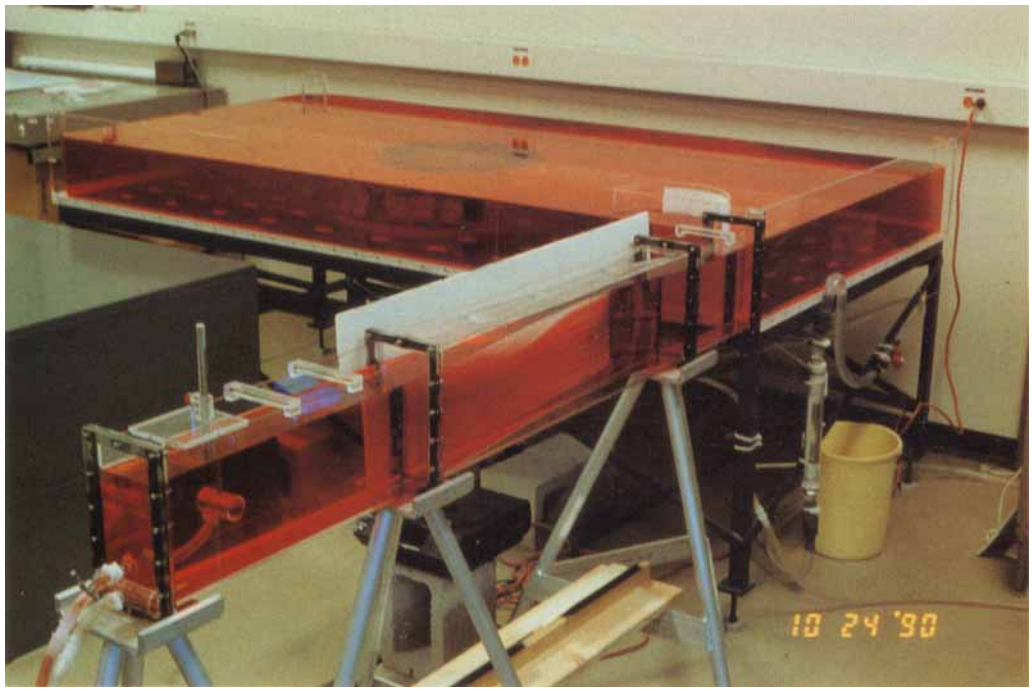

FIGURE 1. Overview of the experimental facility, showing the rectangular stratified reservoir in the background, the convergent–divergent channel in front of the white screen and the withdrawal sinks in the foreground.

(a)

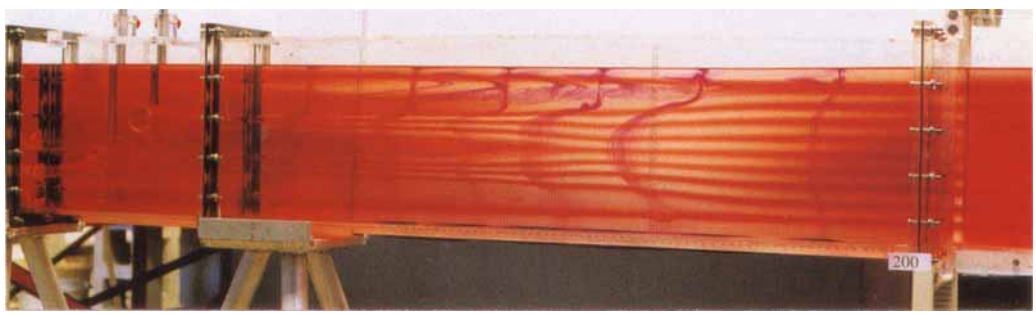

(b)

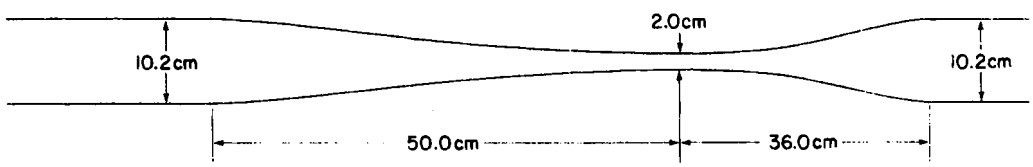

FIGURE 2. *(a)* Details of the contraction, the downstream section of the channel and the withdrawal sinks. *(b)* Top view of the convergent–divergent section of the channel drawn to scale.

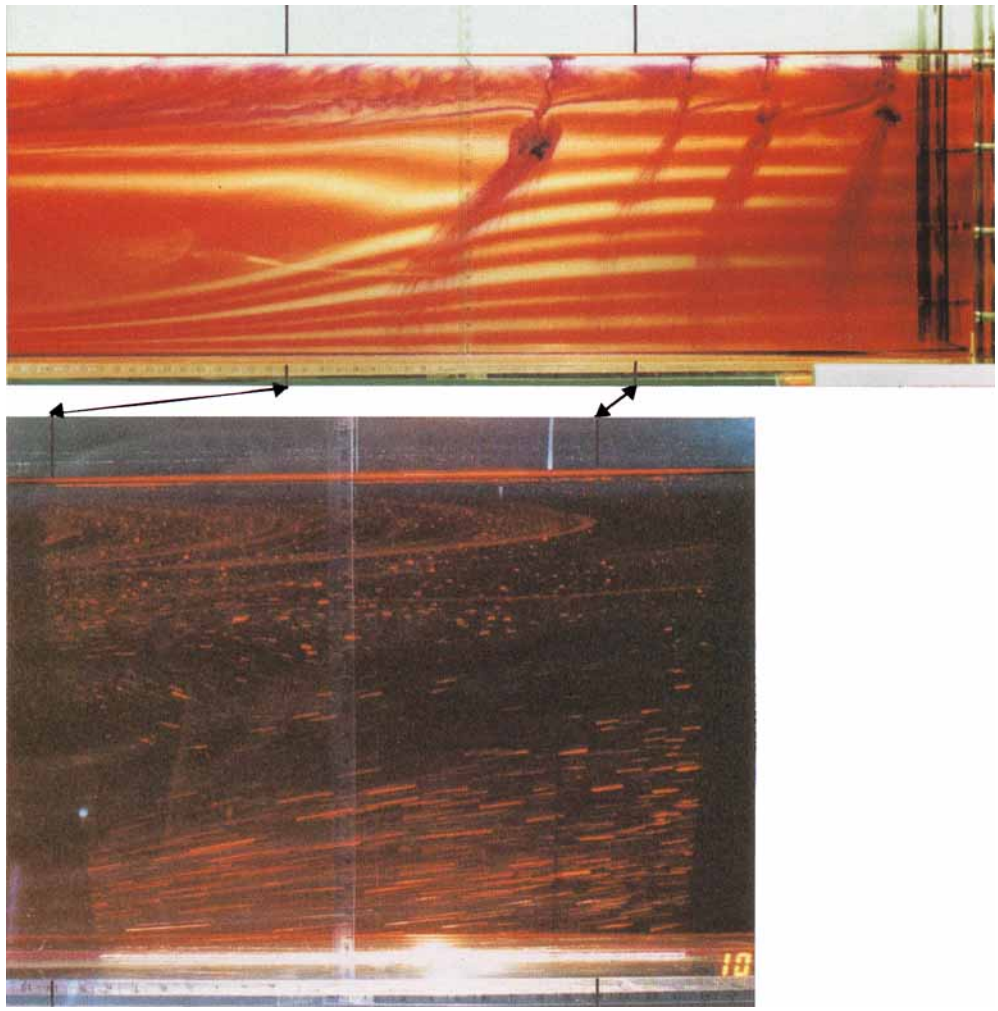

FIGURE 3. *(a)* Internal self-similar flow (structure 1) with the withdrawal slit at the bottom of the channel. *(b)* Streak photograph of a portion of the flow, indicated by the inset lines, shown in *(a)*.

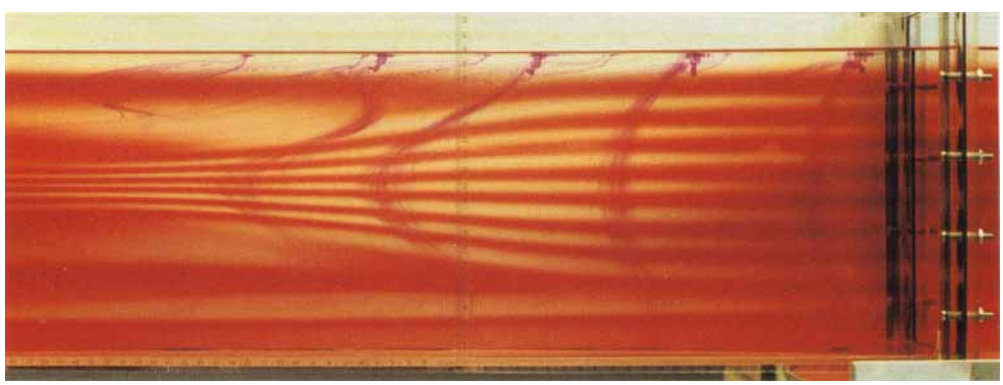

FIGURE 6. Internal self-similar flow (structure 2) with the withdrawal slit 11.5 cm above the bottom of the channel.

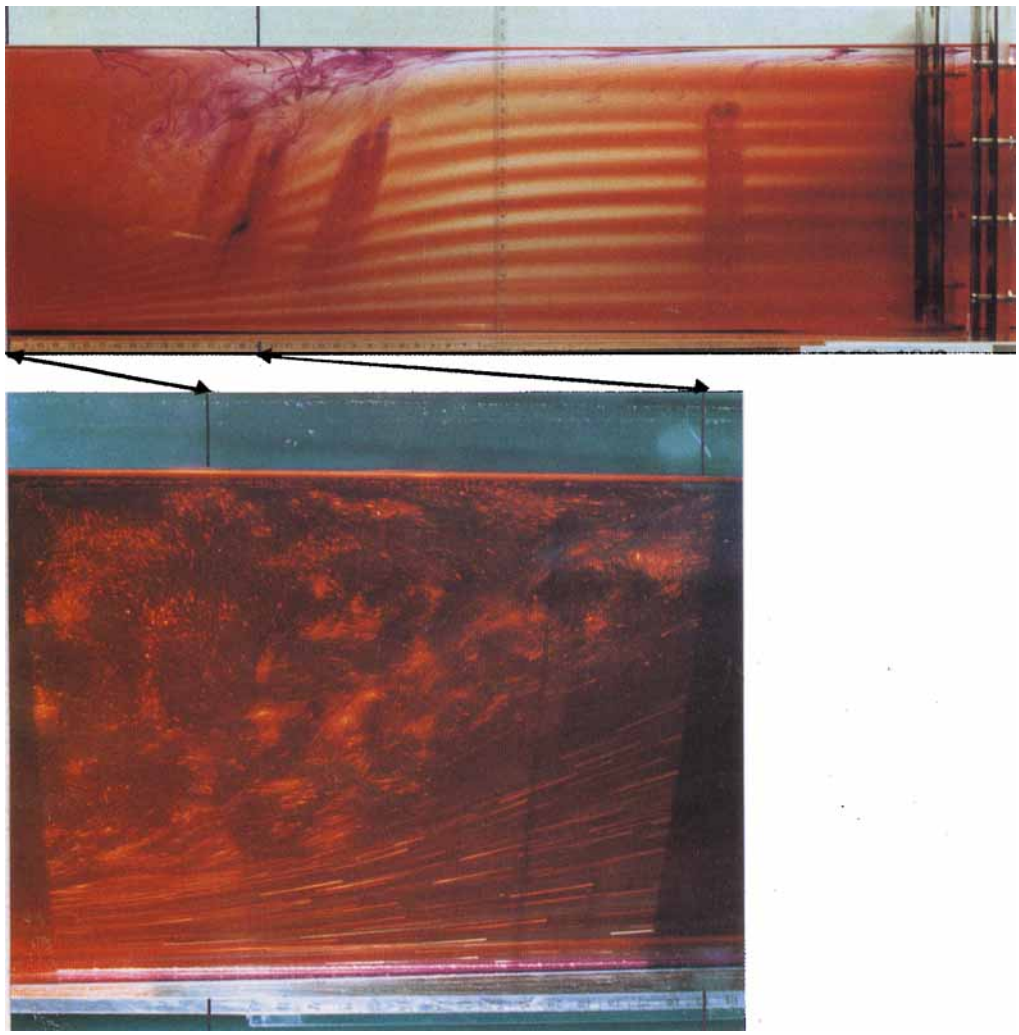

FIGURE 7. *(a)* Enclosed self-similar flow with nearly uniform flow upstream. In the divergent section the structure-1 flow has a separation isopycnal, remains supercritical and flows into a withdrawal slit at the bottom of the channel. *(b)* Streak photograph of a portion of the flow, indicated by the inset lines, shown in *(a)*.

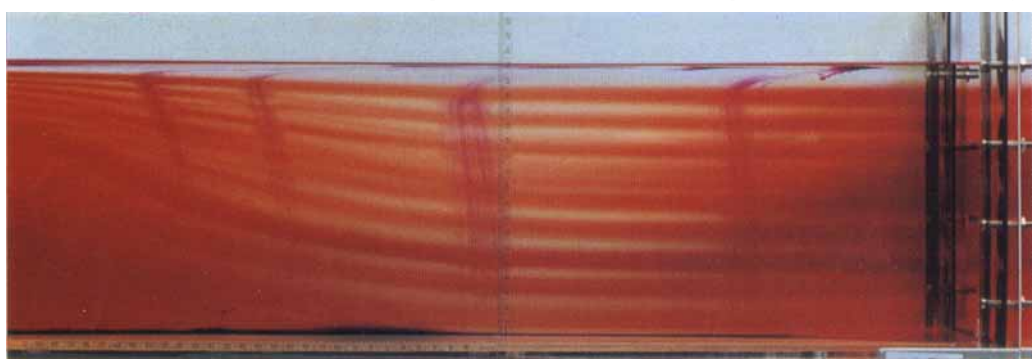

FIGURE 9. Enclosed self-similar flow with nearly uniform flow upstream. In the divergent section the structure-1 flow has a separation isopycnal, remains supercritical and flows into a withdrawal slit at the top of the channel. The flow is an inverted version of the flow in figure 7*(a)*.

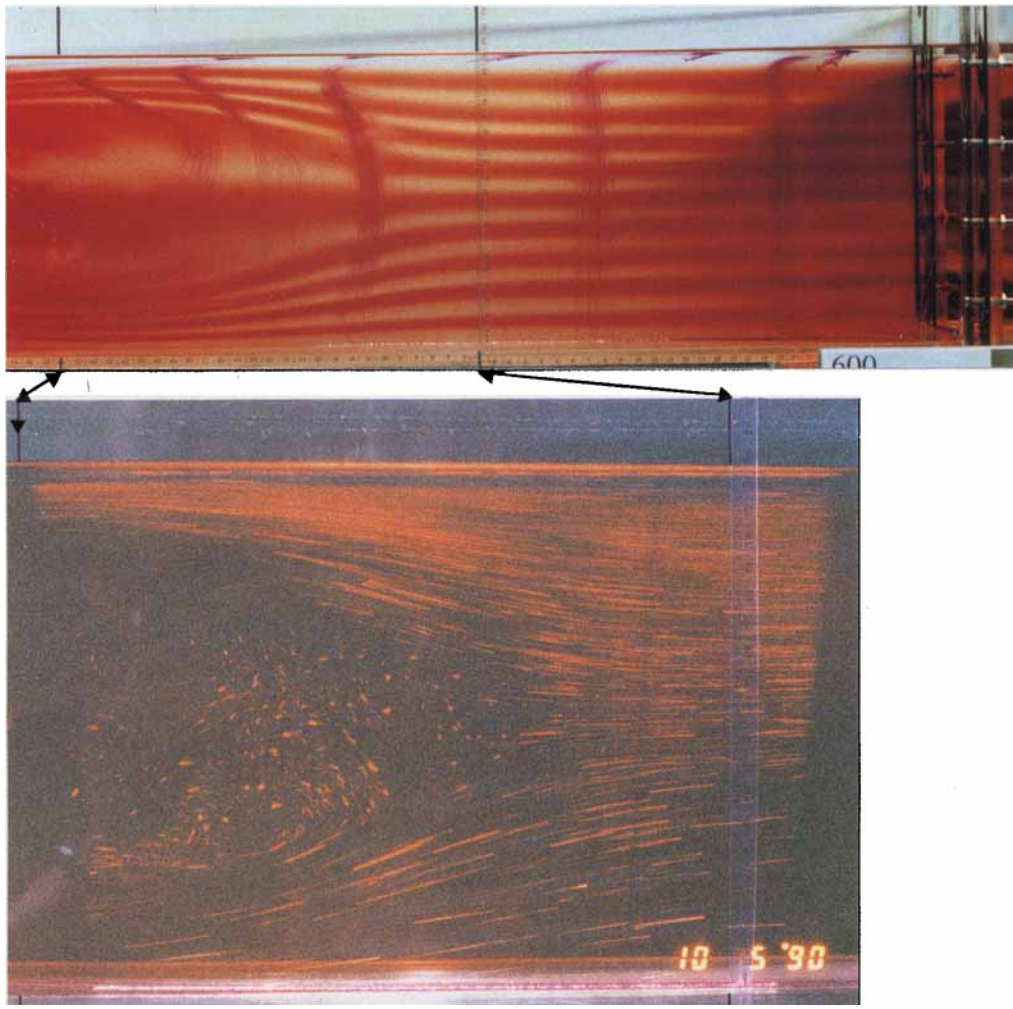

FIGURE 15. *(a)* Enclosed self-similar flow with nearly uniform flow upstream. In the divergent section the structure-2 flow has a separation isopycnal, remains supercritical and flows into withdrawal slits at the top and bottom of the channel. *(b)* Streak photograph of a portion of the flow, indicated by the inset lines, shown in *(a)*.

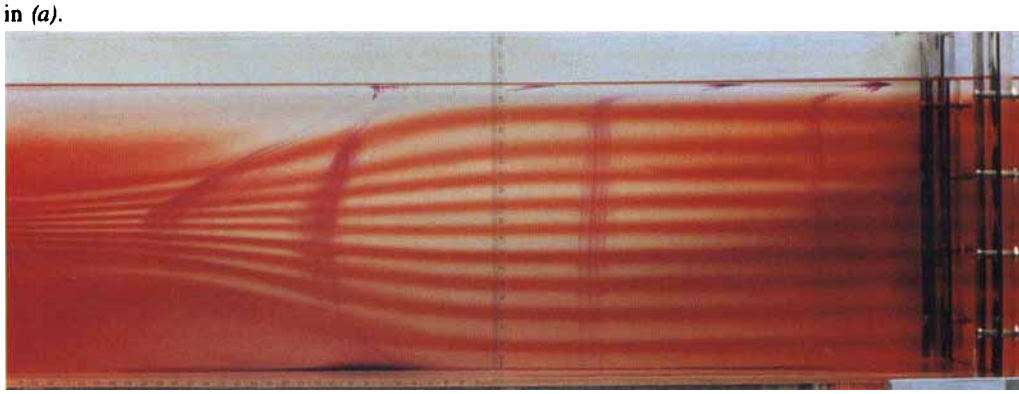

FIGURE 17. Enclosed self-similar flow with nearly uniform flow upstream. In the divergent section the structure-2 flow has a separation isopycnal, remains supercritical and flows into a withdrawal slit at the centre of the channel.

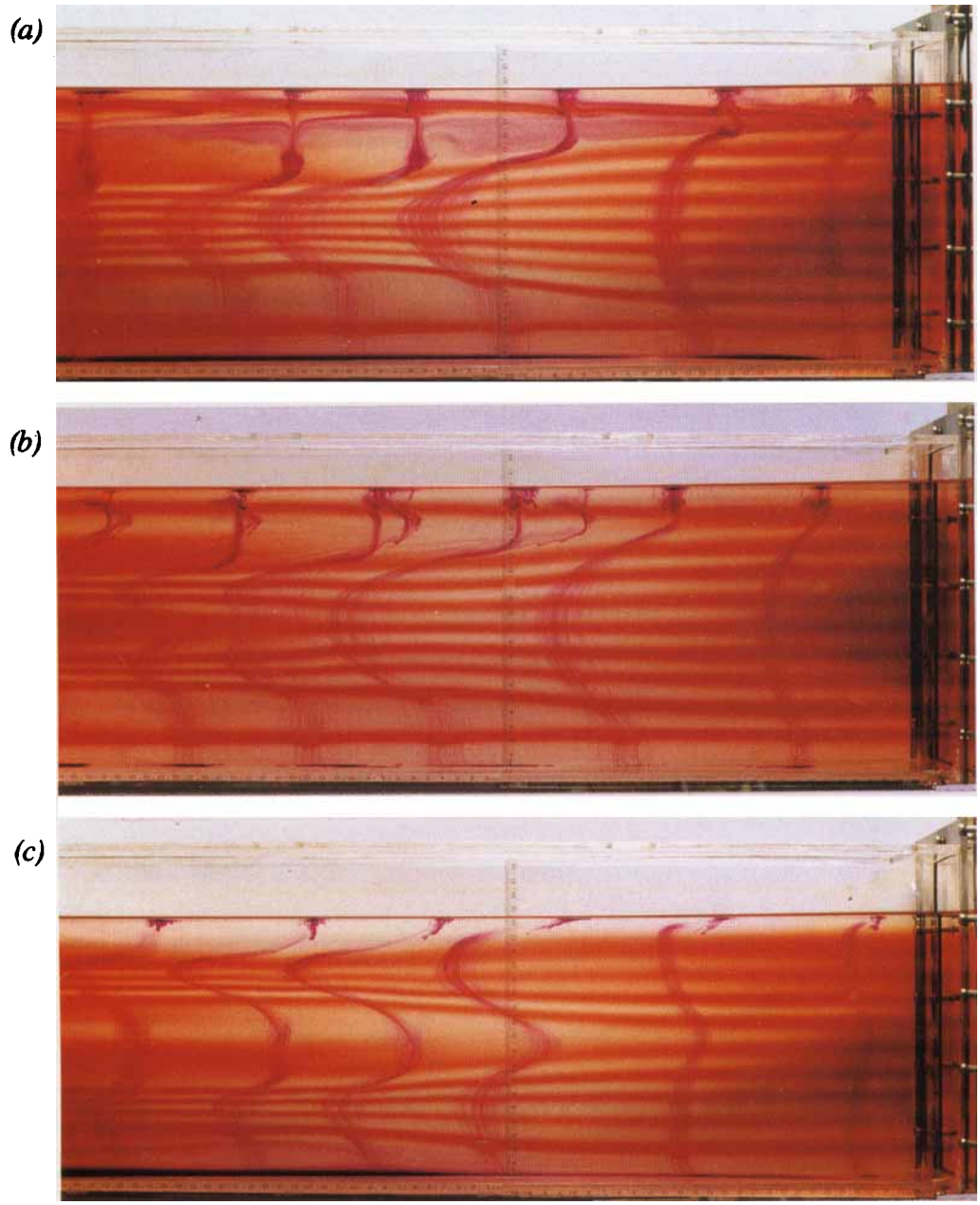

FIGURE 18. *(a)* Internal self-similar flow controlled at the narrowest section. The two downstream withdrawal slits have a vertical separation of 5 cm. *(b)* Subcritical internal self-similar flow controlled downstream with bifurcation to two jets in the divergent section of the channel. The two downstream withdrawal slits have a vertical separation of 7 cm. *(c)* Two separate internal self-similar flows, each controlled at the narrowest section. The two downstream withdrawal slits have a vertical separation of 9.5 cm.

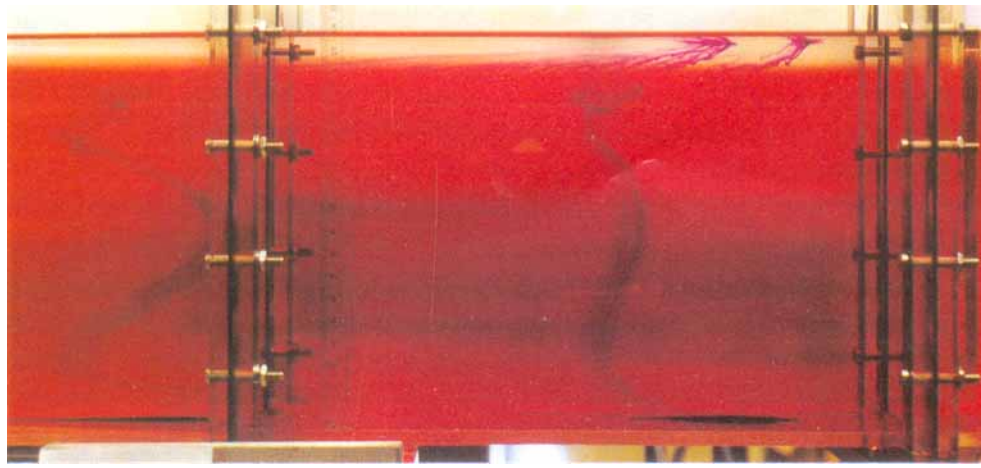

FIGURE 10. Flow in a region of constant channel width close to the reservoir. Vertical dye streaks show top and bottom boundary layers and small velocity defect at mid-depth.

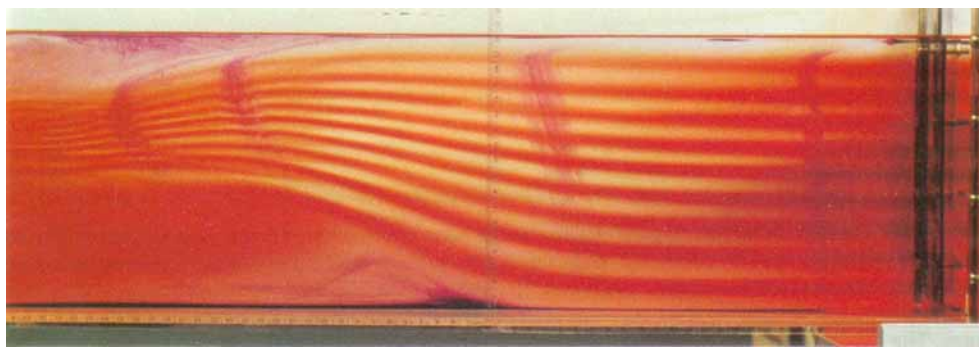

FIGURE 19. Subcritical internal self-similar flow controlled downstream with bifurcation to two jets in the divergent section of the channel. The two downstream withdrawal slits are at the bottom of the channel and 7 cm above the bottom of the channel.

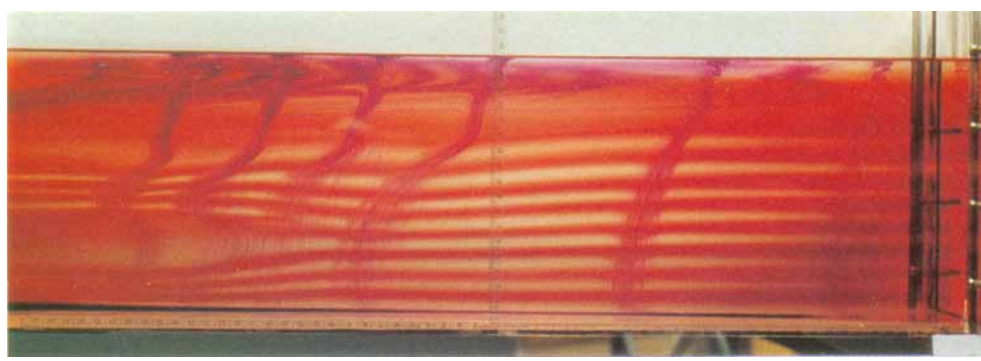

FIGURE 20. Separating flow with the withdrawal slit 12 cm above the bottom of the channel.

We want to find reservoir functions $f(z)$ that allow a solution to connect smoothly from the reservoir to the narrowest point in the channel. The self-similar solution has the form

$$y = k(\lambda)\, z. \tag{9}$$

The relationship between density surface height and channel width $k(\lambda)$ is found by applying the upper boundary condition (8*b*). Using the self-similar solution (9) in the upper boundary condition (8*b*), we find $\lambda k^2(1-k) = f(z_0)/2\Delta\rho z_0$, a constant. The narrowest section, where $\lambda = 1$, is a minimum value of λ and so $\mathrm{d}\lambda/\mathrm{d}k = 0$, which leads to

$$\lambda(k^2 - k^3) = \tfrac{4}{27} \tag{10}$$

and (6) becomes

$$f(z) = \frac{8}{27}\left(\Delta\rho\, z_0 - \int_z^{z_0} \rho' \hat{z}\, \mathrm{d}\hat{z}\right). \tag{11}$$

This solution, with $\Delta\rho = 0$, was first found by Wood (1968), and has also been discussed by Yih (1969), who showed that it is one of a class of stratified flows, governed by a model based on the shallow-water approximation, whose stream surfaces duplicate those found for the corresponding flow of a homogeneous fluid. Benjamin (1981) generalized Wood's result to the form given here and went on to show that the self-similar solution is critical at the narrowest section with respect to small long-wave disturbances of the lowest mode and is supercritical with respect to all long-wave modes in the divergent section of the channel.

The self-similar solution is the only solution to (8*a*, *b*) that has been found. In a continuously stratified reservoir, for a particular flow rate, a range of densities $\rho(0)$ to $\rho(z_0)$ flows from the reservoir. As the flow rate changes, the flow remains self-similar while the range of densities drawn from the reservoir changes so that the flow at the narrowest section remains critical with respect to the lowest wave mode. Since this flow withdraws fluid from a limited range of densities, we call it an internal self-similar flow.

2.3. *Comparison of the internal self-similar solution with experiments*

Velocity profiles measured at the narrowest section and 10 cm upstream and downstream of the narrowest section are shown in figure 5(*a–c*) for the flow shown in figure 3(*a*, *b*). The theoretical self-similar velocity profile is also shown as a solid line.

Throughout the channel, the theory predicts a velocity profile that is somewhat thinner and faster than observed, primarily an effect of the sidewall boundary layers. These boundary layers become thicker with downstream position and effectively move the most constricted section downstream of the narrowest section; the effective width at this section is also smaller than the measured width. In the vicinity of the narrowest section, the height of the density surfaces and the velocity profile are sensitive to variations in channel width and hence also the thickness of the sidewall boundary layers. Nonetheless, the global structure of the flow is accurately predicted by the theory; only the downstream displacement of this structure, due to the sidewall boundary layers, is sensitive to frictional effects. This also occurs in single-layer hydraulics.

While the detailed structure of the boundary layers in the accelerating flow is beyond the scope of this work, a correction for their effect on the internal hydraulics can be made. Using the relationship

$$Q_{\text{total}} = \tfrac{1}{6}\pi z_0^2\, b_n\, (-g\rho'/\rho_0)^{\frac{1}{2}}$$

from (7) and (11), the total volume flux Q_{total} and the observed depth of the moving fluid far upstream z_0 are used to calculate the effective width of the channel at the narrowest point b_n; ρ_0 is the density and ρ' is the density gradient at the upstream

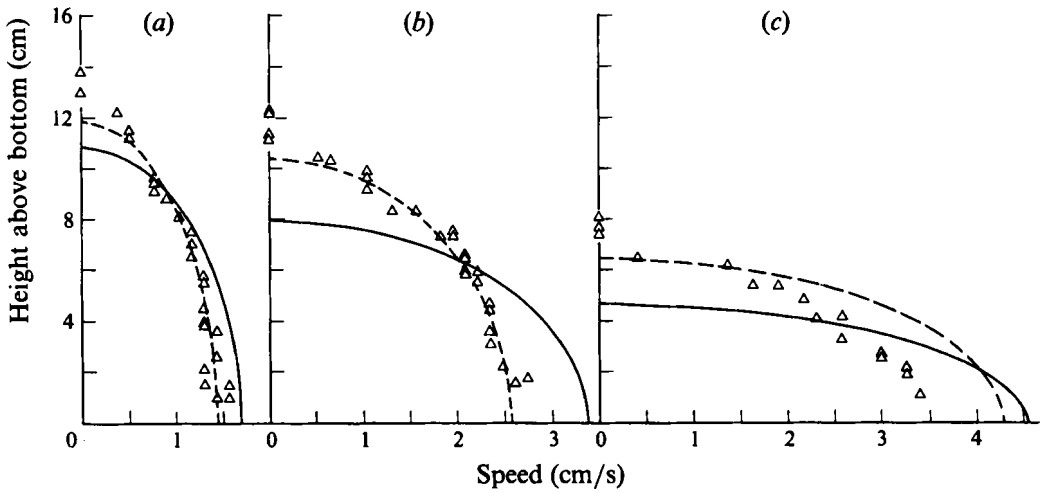

FIGURE 5. Velocity profiles for the internal self-similar flow (structure 1) shown in figure 3(*a*). (*a*) 10 cm upstream of the narrowest section, channel width $b = 2.9$ cm, non-dimensional channel width $b' = 1.45$, channel width parameter $\Delta\beta/\pi = 0.47$. (*b*) At the narrowest section, $b = 2.0$ cm, $b' = 1$, $\Delta\beta/\pi = 0$. (*c*) 10 cm downstream of the narrowest section, $b = 2.5$ cm, $b' = 1.25$, $\Delta\beta/\pi = 0.26$. The solid line shows the theoretical self-similar velocity profile, and the dashed line shows the self-similar velocity profile for the actual measured depths of the flow.

reservoir. The total depth of the moving fluid at each of the three stations shown in figure 5 is then used to calculate the effective width at these stations. Finally, the actual channel width at these stations is known and the effective boundary-layer thickness can be compared with that estimated from laminar boundary-layer theory.

For the experiment shown in figures 3 and 5, an upstream depth of 12.7 cm gives an effective most constricted width of 1.6 cm. This effective most constricted width occurs where all the isopycnals of the self-similar flow have dropped to two thirds of their individual reservoir heights. Inspection of figure 3 shows this to occur for this flow about 5 cm downstream of the narrowest section. For the measurement stations, boundary-layer thicknesses of 0.5, 1 and 4 mm are needed to give the depths shown in figures 5(*a*), 5(*b*), 5(*c*) respectively. These are in agreement with a boundary-layer thickness scale, $\delta^2 = \nu L/U$; with $U = 2$ cm/s and $L = 20$ cm, $\delta = 3$ mm. It is beyond the scope of the present work to compute the thickness of the boundary layer in the convergent–divergent contraction. The dashed lines in figure 5(*a–c*) show the self-similar velocity profiles for the measured depths of this flow. The agreement between the correction for sidewall boundary layers and the measured velocities is good for the stations in the convergent and narrowest sections. In the divergent section, figure 5(*c*), the correction underestimates the velocities and total transport by approximately 20%. Here, in spite of the fact that the expansion is extremely gradual with a tangent of less than 5% (figure 2*b*), the sensitivity to this tangent when the flow is close to critical results in isopycnal slopes as large as 15°. The vertical velocity component is about a quarter of the horizontal component; hence some of the vertical displacement of the isopycnals has gone into this component of the kinetic energy. From the energetics alone this amounts to a horizontal velocity error of about 10%. Also, as the flow accelerates in the divergent section a weak velocity field is induced above the separation isopycnal due to viscosity at the interface.

A different internal self-similar flow, obtained by withdrawing fluid from 11.5 cm above the base of the channel, is shown in figure 6 (plate 2). The moving region is now bounded both above and below by stagnant fluid and the vertical dye lines show a

structure-2 velocity profile, having a velocity maximum at the centre of the region of moving fluid. The thickness of the withdrawn region is controlled by the total volume flux, and the vertical position of the withdrawn fluid is controlled by the height of the sink. The dye lines show that, as in the structure-1 flow discussed above, the vertical extent of the velocity field is greater than is apparent from observing the range of isopycnals that form the rapidly moving jet in the divergent section of the channel.

2.4. *Enclosed self-similar solutions*

As the flow rate increases, the self-similar flow draws fluid from an increasingly large range of densities. There is a critical flow rate above which fluid at all depths is drawn from the reservoir, and $\Delta\rho$ is then the density step at the free surface. In this situation, if the density variation within the fluid is small and the density step at the free surface is approximately equal to the mean density of the moving fluid, the first term in (11) dominates the reservoir function of the self-similar solution and the flow is nearly vertically uniform at every section of the channel. The speed of the lowest mode barotropic wave is much greater than the speeds of the baroclinic modes, and as long as the fluid velocities are much less than this barotropic wave speed, our attention can be restricted to internal hydraulics by assuming that the free surface is level. If we in addition make the Boussinesq approximation, the governing equation (8*a*) is unchanged, the boundary conditions (8*b*) become

$$y(0) = 0 \quad \text{and} \quad y(z_0) = z_0 \tag{12}$$

and the self-similar solution, now called an enclosed self-similar flow, is

$$y = z \tag{13a}$$

and

$$f = \rho_0 q^2 / g b_n^2. \tag{13b}$$

The reservoir function and the flow rate per unit depth are both constant, and ρ_0 is the mean density of the fluid. In this approximate solution, the density surfaces are horizontal as the fluid flows through the contraction, and the fluid velocity,

$$u = q/b, \tag{14}$$

is vertically uniform at any point along the channel. The solution is symmetric about the narrowest section; if the solution were to exist in the divergent section, it would simply decelerate with level stream surfaces just as the solution in the convergent section accelerates.

2.5. *Enclosed self-similar flows*

A flow of this type is shown in figure 7(*a*) (plate 3), in which fluid was withdrawn from a slit at the bottom of the channel. For now, we will only discuss the flow in the convergent section of the channel, which is on the right-hand side of the photograph. The vertical dye line and horizontal isopycnals upstream of the narrowest section show that fluid at all depths is flowing into the contraction and that the flow is vertically nearly uniform apart from the top and bottom boundary layers. The velocity profile 10 cm upstream of the narrowest section, shown in figure 8(*a*), also shows that the velocity in the convergent section of the channel is vertically nearly uniform.

As with the internal self-similar flow, the enclosed flow passes through an infinite sequence of virtual controls as it flows from the stagnant reservoir into the channel and these controls determine the vertical structure of the flow. However, at the narrowest section this flow is supercritical with respect to all the internal modes while the free-surface mode is very subcritical and hence acts as a rigid lid. Information about the vertical structure of the downstream conditions cannot propagate through the contraction and only the free surface level and total flow rate are controlled

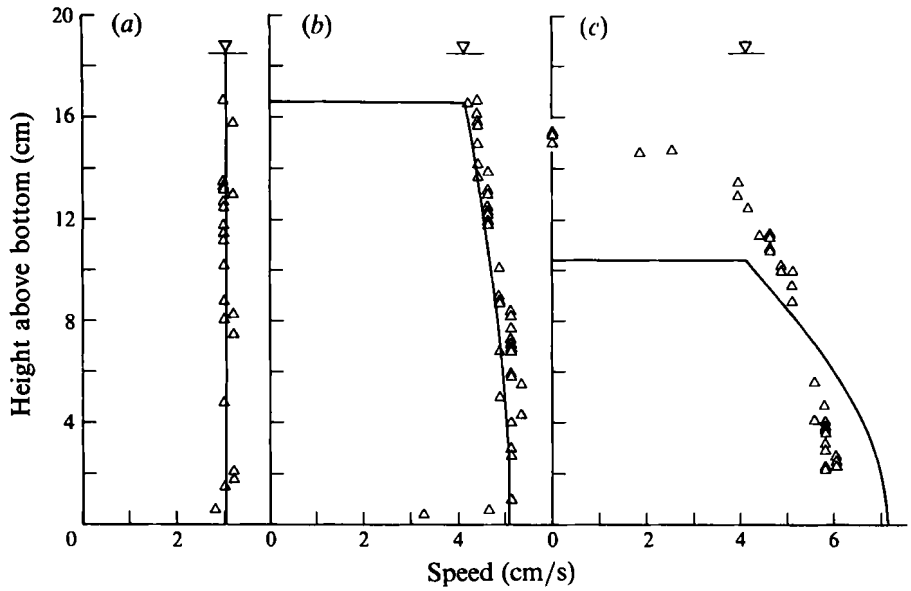

FIGURE 8. Velocity profiles of the enclosed self-similar flow with structure-1 separating flow in the divergent section shown in figure 7(*a*). (*a*) 10 cm upstream of the narrowest section, $b = 2.9$ cm, $b' = 1.45$, $\Delta\beta/\pi = 0.28$. (*b*) At the narrowest section, $b = 2.0$ cm, $b' = 1$, $\Delta\beta/\pi = 0$, $\beta_n = 0.62\pi$. (*c*) 10 cm downstream of the narrowest section, $b = 2.5$ cm, $b' = 1.25$, $\Delta\beta/\pi = 0.16$.

downstream; the flow in the convergent section of the channel is independent of the downstream conditions. Figure 9 (plate 3) shows a flow similar to that of figure 7(*a*) but with the withdrawal slit at the top of the channel instead of at the bottom. The vertical dye line in the convergent section of the channel again shows a vertically uniform flow, clearly showing that in the convergent section, these flows are independent of the downstream conditions. For the stratifications considered here, the predicted velocity difference between the top and bottom of the channel is less than 1%, and so we will use the Boussinesq theory when making comparisons between theory and experiments. Notice that the uniform velocity profile is the same as the upstream conditions used by Long (1955) when studying experimentally flow over a towed ridge, but here the velocity profile is determined by the series of virtual controls rather than being prescribed.

An interesting experimental aside was observed in the convergent section of the channel. Departure from vertically uniform flow is obvious in the boundary layers at both the free surface and at the bottom of the channel. In the slow moving region close to the reservoir, these boundary layers cause a significant variation in the whole of the vertical velocity profile that can be explained by arguments similar to those used to study frictional effects in conventional open channel flows. Figure 10 is a photograph of vertical dye lines in a parallel-sided section of the channel that is about five times the width of the narrowest section and is located in the convergent part of the channel. (Figures 10, 19 and 20 are on plate 6, a plate showing figures outside of the main thrust of the paper.) The flow rate is such that this is an enclosed self-similar flow, so the velocity profile in the convergent section is theoretically nearly uniform. At a particular streamwise location in the subcritical portion of the flow, frictional effects require the flow to have more potential energy and less kinetic energy than the frictionless theory would predict. It is also necessary for the total energy to be greater than that predicted by frictionless theory, the excess being dissipated in the boundary layers as the flow

moves through the contraction. In a single-layer flow this means that the flow is slower and deeper than otherwise predicted. In the flow shown here, the boundary layers are approximately vertically symmetric and so are to first order a second mode effect. This suggests that when the flow is subcritical with respect to the second mode, as in the wide channel shown in figure 10, there will be less kinetic energy and more potential energy in this mode than theoretically predicted. Lower kinetic energy in this mode explains both the velocity defect in the centre of the channel and the smoothness of the velocity profile seen in figure 10. Effects of the increased potential energy, in principle observable by slightly displaced isopycnals, were not seen. Owing to the constraint imposed by the mode-2 virtual control, upstream of this virtual control the boundary layers have a pronounced effect on velocities at all depths.

3. Separating isopycnals: deceleration towards a virtual control

If the density surfaces remained level in the divergent section of the channel, the enclosed self-similar flow would simply decelerate in the divergent section. This flow would be symmetric about the narrowest section and the flow would become subcritical with respect to various internal modes as the channel diverged. However, we are studying flows with highly non-uniform downstream conditions and so this does not happen. Similarly, in the two-layer virtually controlled experiments of Armi (1986), the flows in the convergent section of the channel were uniform, but in the divergent section always remained supercritical and accelerated either the upper or lower layer.

For the flow shown in figure 7(*a*), with the withdrawal point at the bottom of the channel, the flow remains supercritical with respect to the lowest internal mode in the divergent section of the contraction. Downstream of the narrowest section, the moving fluid separates at the upper boundary and flows below a region of nearly stagnant fluid, forming a fast moving supercritical flow on the bottom of the channel. This flow is sheared, with higher velocities at the bottom of the channel, and is not self-similar. There is a transition from a structure-0 flow in the convergent section to a structure-1 flow in the divergent section. A streak photograph of a part of this flow in the divergent section is shown in figure 7(*b*).

3.1. *Bifurcations of the enclosed self-similar solution*

We now look for bifurcations of the self-similar solution at some point in the channel, giving a non-self-similar solution downstream of the bifurcation point. In the two-layer system, solutions of this nature have been found and demonstrated by Armi (1986). We will examine this possibility in the enclosed, continuously stratified Boussinesq system, in which the fluid velocity is vertically uniform within the self-similar flow. We seek solutions that are controlled and asymmetric about the narrowest section. The solutions will have uniform flow upstream of the bifurcation point but will be non-uniform downstream of that point. This will allow different upstream and downstream reservoirs to be linked, although the question of the form of the internal hydraulic jump that typically occurs to connect the supercritical flow in the divergent part of the channel to the subcritical downstream reservoir condition is not considered here.

The governing equation (8*a*) is rewritten as

$$2fy''-f'y'-2\lambda\rho'y'^3(y-z)=0 \tag{15}$$

and the boundary conditions are given by (12). Since the enclosed self-similar solution is $y=z$, the problem is restated in terms of the deviation from this solution:

$$w(z)=y-z. \tag{16}$$

Since f is constant in the enclosed self-similar solution, the following are obtained upon substitution of (16) into (15) and (12):

$$w''-(\lambda\rho'/f)\,w(w'+1)^3=0, \tag{17a}$$

$$w(0)=0 \quad \text{and} \quad w(z_0)=0. \tag{17b}$$

Equation (17a) will now be transformed so that the local stream surface height y is the independent variable. The definition of w, (16), is used to obtain

$$\frac{\mathrm{d}w}{\mathrm{d}z}=\frac{\mathrm{d}w}{\mathrm{d}y}\frac{\mathrm{d}y}{\mathrm{d}z}=\frac{\mathrm{d}w}{\mathrm{d}y}\left(1+\frac{\mathrm{d}w}{\mathrm{d}z}\right)$$

and

$$\frac{\mathrm{d}^2w}{\mathrm{d}z^2}=\frac{\mathrm{d}^2w}{\mathrm{d}y^2}\left(1+\frac{\mathrm{d}w}{\mathrm{d}z}\right)^3,$$

and so the problem becomes

$$\frac{\mathrm{d}^2w}{\mathrm{d}y^2}-\frac{\lambda\rho'}{f}w=0, \tag{18a}$$

$$w(0)=0 \quad \text{and} \quad w(y_0)=0, \tag{18b}$$

in which $w=w(y)$ but ρ' is in general a function of z, and hence a function of $(y-w)$.

We will now restrict our attention to a linear density profile and will non-dimensionalize the problem, using the reservoir depth z_0 as the vertical scale for w and y. The governing equation (18a) for the deviation in the height of a stream surface from its upstream value becomes

$$\frac{\mathrm{d}^2w}{\mathrm{d}y^2}+\beta^2w=0 \tag{19a}$$

along with the boundary conditions

$$w(0)=0, \quad w(1)=0. \tag{19b}$$

The channel width and flow rate are represented by the parameter

$$\beta^2=-g\rho' b^2z_0^2/\rho_0 q^2, \tag{20}$$

which is independent of y. Equation (19a) is similar to the shallow-water approximation of the governing equations derived by Long (1953) when studying flow over a ridge. The difference is that here β depends on the local channel width as well as the upstream conditions and so the topographic variability enters the governing equation rather than the boundary conditions, as occurs in the study of flow over a ridge. Note that β is an inverse bulk Froude number and when $w=0$, the velocity is given by (14) and so

$$\beta^2=-g\rho' z_0^2/\rho_0 u^2. \tag{21}$$

The solution to (19) is

$$w(y)=A\sin\beta y+B\cos\beta y. \tag{22}$$

The lower boundary condition gives $B=0$ and the upper boundary condition gives $\beta_m=m\pi$ where m is a positive integer, and so β is constant in any non-trivial solution. Note that the β_m give the positions of the virtual controls of the enclosed self-similar flow. Since β is related to the channel width and is constant in all non-trivial solutions, there are no solutions away from the virtual controls other than the flow with level stream surfaces, in which $w=0$ everywhere.

The form of non-trivial solutions of (19) that exist at more than an isolated value of β are suggested by the solutions for the flow over a ridge of a linearly stratified Boussinesq fluid found by Smith (1985). To study flow through a contraction we, like

Smith, introduce a layer of stagnant fluid of constant density at the top of the channel and look for a solution with the moving fluid at the bottom of the channel, as shown in figure 7(*b*). An analogous inverted problem is obtained by introducing the stagnant layer at the bottom of the channel as in figure 9: which flow actually occurs depends on the downstream conditions. We call the point at which the stagnant-layer thickness is zero the separation point as in Armi & Farmer (1986) and Williams & Armi (1991); we assume that the pressure at the separation point is hydrostatic since the front associated with the stagnant fluid is wedge like. This will be a reasonable approximation as long as the channel geometry is such that the slope of the density surfaces downstream of the separation point is small.

Downstream of the separation point, the moving and non-moving regions are separated by a dividing streamline, and the deflection of this streamline from the upstream height $z = 1$ is given by w_0. Thus the stagnant-layer thickness is $-w_0$ and $w_0 \leqslant 0$ everywhere. The continuity equation (5) is used to find that the velocity downstream of the separation point is

$$u(y) = u_s \frac{\beta_s}{\beta}\left(1 - \frac{\mathrm{d}w}{\mathrm{d}y}\right), \tag{23}$$

where subscript s refers to values at the separation point. The problem is now one of matching the self-similar flow to the separated flow and, downstream of the separation point, finding the height of the separation streamline.

A new boundary condition applies on the separation streamline at the top of the moving fluid. This is found by considering Bernoulli's equation and the continuity condition on the streamline. At the separation point, the velocity at the free surface is u_s and at some downstream location, the velocity is u. Applying Bernoulli's equation along the streamline gives $u = u_s$. Using this result in (23) evaluated at the separation streamline, we find that the boundary condition at the top of the moving fluid is

$$w_y(y_0) = 1 - \beta/\beta_s. \tag{24}$$

We also define the change in height of the dividing streamline as

$$w(y_0) = w_0, \tag{25}$$

while the lower boundary condition remains

$$w(0) = 0. \tag{26}$$

Applying (26) to the general solution (28) gives

$$w(y) = A \sin \beta y. \tag{27}$$

The two conditions at the upper boundary, (24) and (25), are then used to find

$$\tan[\beta(w_0 + 1)] = w_0 \beta \beta_s/(\beta_s - \beta), \tag{28a}$$

$$A = w_0/\sin[\beta(w_0 + 1)]. \tag{28b}$$

The streamwise derivative of (28*a*) at the narrowest section (where $\mathrm{d}\lambda/\mathrm{d}x = 0$) gives

$$\frac{\mathrm{d}w_{0n}}{\mathrm{d}x}(\beta_n w_{0n} - \tfrac{1}{2}\sin[2\beta_n(1 + w_{0n})]) = 0, \tag{29}$$

where β_n and w_{0n} are the values of β and w_0 at the narrowest section. A solution will be asymmetric about the narrowest section if $\mathrm{d}w_{0n}/\mathrm{d}x \neq 0$, and (29) then requires that

$$\beta_n w_{0n} = \tfrac{1}{2}\sin[2\beta_n(1 + w_{0n})]. \tag{30}$$

Using (28*a*), β_s is then found to be

$$\beta_s = \beta_n/\sin^2[\beta_n(1 + w_{0n})]. \tag{31}$$

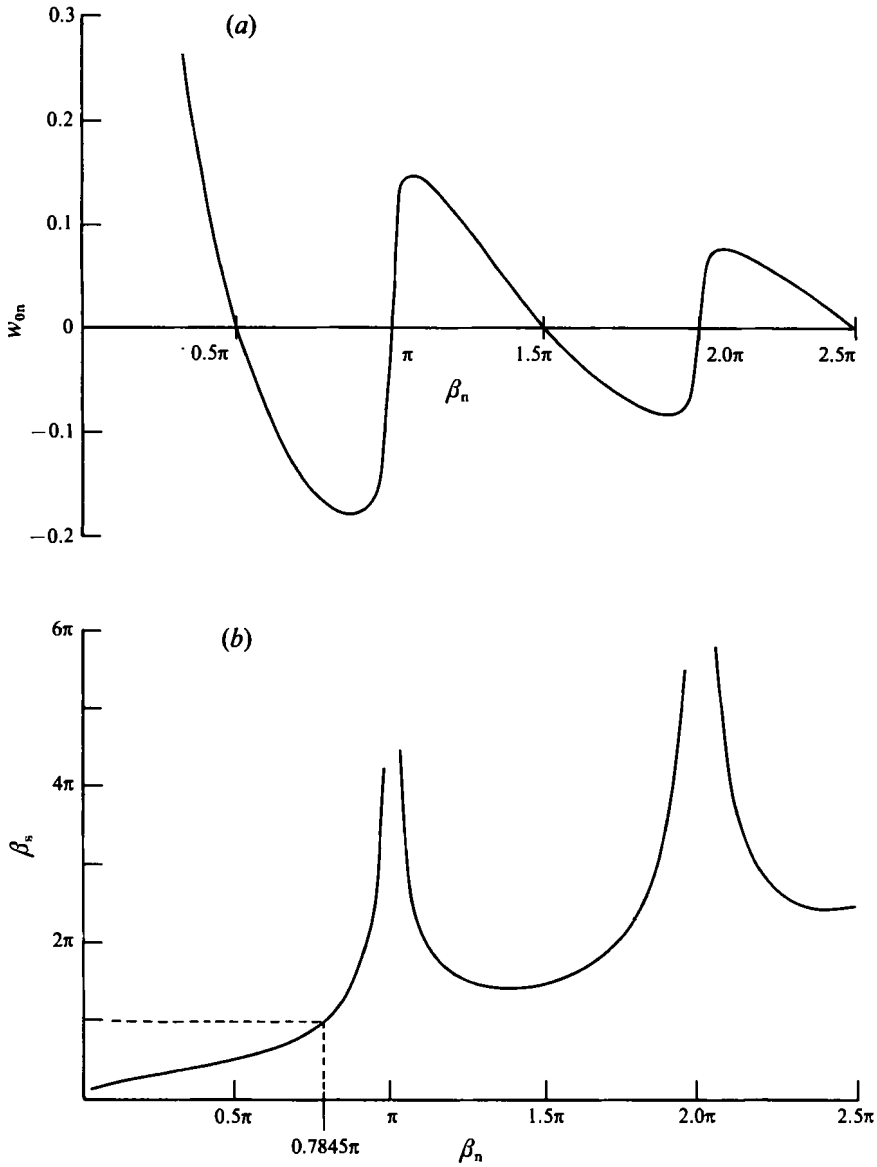

FIGURE 11. (*a*) w_{0n} *vs.* β_n: deviation of dividing streamline *vs.* the channel width parameter, evaluated at the narrowest section, from (30). (*b*) β_s *vs.* β_n: channel width parameter at the separation point *vs.* the channel width parameter at the narrowest section, from (31).

For a particular minimum channel width, (30) allows w_{0n}, the stagnant layer depth at the narrowest section, to be found and then (31) determines β_s, the channel width at the separation point. This allows us to find all possible solutions with w_0 asymmetric about the narrowest section. Notice that $w_{0n} \leqslant 0$ in all physically realizable solutions.

Equations (30) and (31) are plotted in figure 11 (*a*, *b*). If one considers a channel of fixed dimensions and a fluid of fixed depth, the definition of β, (20), shows that increasing values of β_n correspond to a decreasing total volume flux. In the range $\frac{1}{2}\pi \leqslant \beta_n < \pi$, the solution can be continued from the separation point to the narrowest section only if $\beta_s < \pi$. Since this is the value of β in the lowest mode solution of (19*a*, *b*), a continuous solution exists only if the uniform flow is critical or supercritical

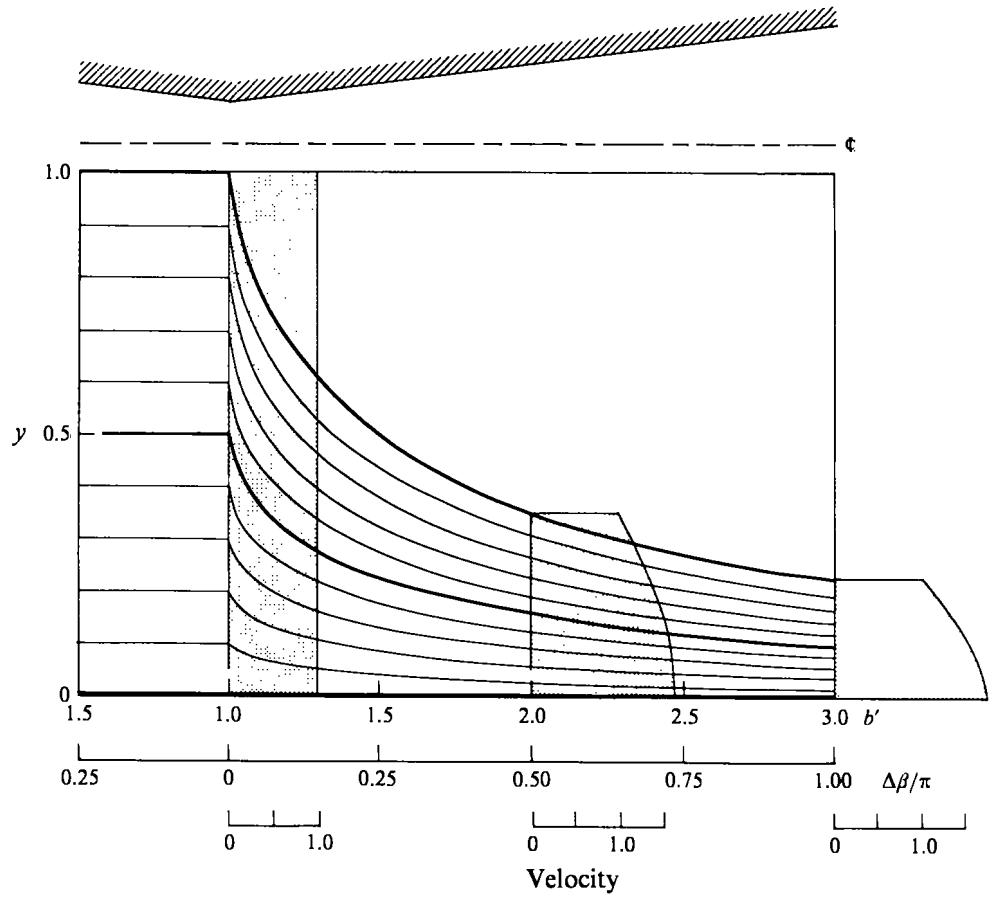

FIGURE 12. Separating flow solution for $\beta_n = \frac{1}{2}\pi$, $\beta_s = \frac{1}{2}\pi$: heights of equally spaced density surfaces and velocity profiles at three locations. The horizontal axis is labelled with $\Delta\beta/\pi$, the change in β from its value at the narrowest section, and with $b' = b/b_n$, the non-dimensional channel width. A plan view of the channel is shown at the top of the figure.

with respect to the gravest internal mode at the separation point; there are solutions from $\beta_n = \frac{1}{2}\pi$, $\beta_s = \frac{1}{2}\pi$ to $\beta_n = 0.7845\pi$, $\beta_s = \pi$. When $\beta_n < \pi$ and $\pi < \beta_s < \frac{3}{2}\pi$, no solutions that smoothly connect the separation point to the narrowest section have been found. When $\beta_s \geqslant \frac{3}{2}\pi$, figure 11(*b*) shows that there are multiple values of β_n for a particular β_s. A solution that smoothly connects the separation point to the narrowest section can only be found for the largest β_n, and so only that β_n represents a real flow.

When $\beta_n < \pi$ and $\beta_s > \pi$, we have not been able to find a solution that matches the enclosed self-similar flow to a separating flow that reaches the narrowest section. Under these conditions, the separation point is upstream of the virtual control of the lowest internal mode so the enclosed self-similar flow is not necessarily the only flow that can come from the stagnant reservoir. It is possible that there are solutions that match a non-self-similar enclosed flow coming from the reservoir to a separating flow upstream of $\beta_s = \pi$ to give a smooth asymmetric solution, but we have not found such a solution.

A separating flow with $\beta_n = \frac{1}{2}\pi$ is shown in figure 12. The separation point occurs at the narrowest section and is also the control point. A separating flow with $\beta_n =$

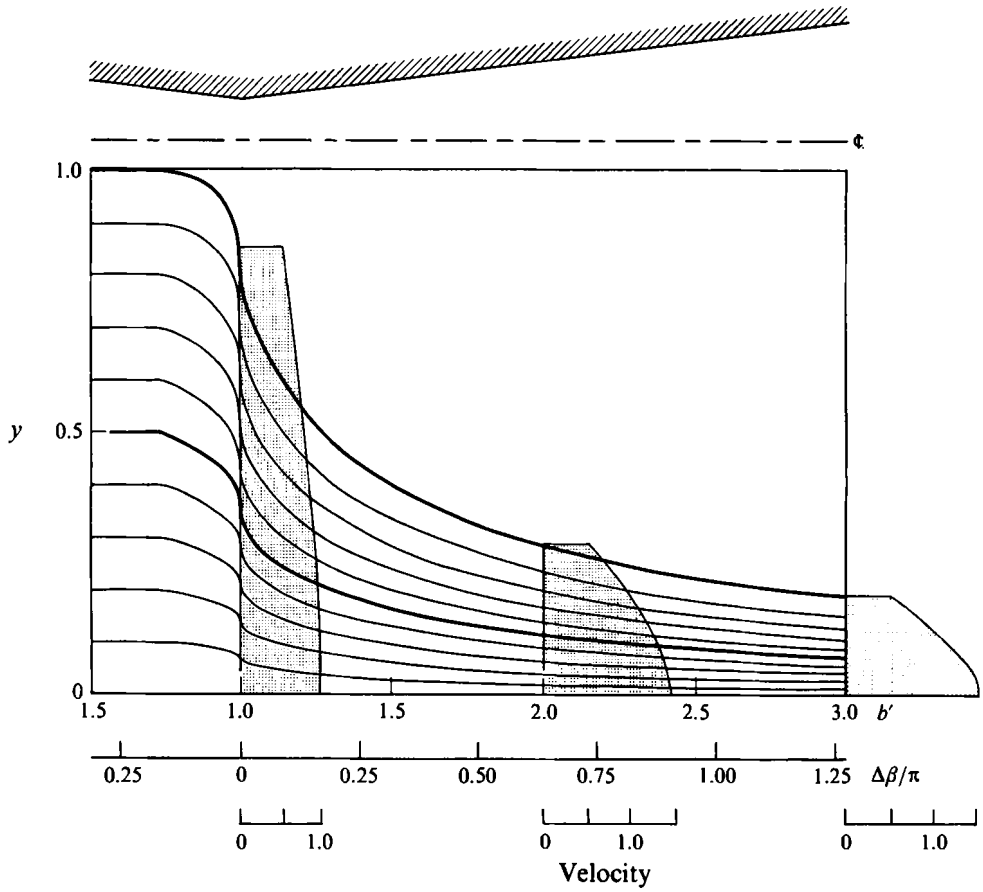

FIGURE 13. As figure 12 but for $\beta_n = 0.7845\pi$, $\beta_s = \pi$.

0.7845π is shown in figure 13. Here, the separation point is upstream of the narrowest section, and the flow is again controlled at the narrowest section. Each solution is shown as the height of various density surfaces and the velocity field at various points in the channel. The velocities are normalized with the velocity at the narrowest section for the flow with $\beta_n = \frac{1}{2}\pi$. In these figures, the channel width varies linearly along the horizontal axis and so in the vicinity of the narrowest section does not represent a slowly varying channel. This gives rise to the rapidly varying density surfaces seen in the figures, which would not occur if the solutions were plotted on a realistic slowly varying channel geometry.

In the separating flow solutions (figures 12 and 13), the density surfaces shown are equally spaced at the separation point but converge more rapidly at the bottom of the moving fluid as the fluid moves downstream and the depth of the moving fluid decreases. Thus the lower part of the moving fluid is accelerated while the velocity at the top remains constant. The density surfaces in the self-similar solution maintain the same relative spacing throughout the channel and, while the magnitude of the maximum velocity increases as the depth of the moving fluid decreases, the velocity profile, like the density profile, is everywhere self-similar.

When $n\pi < \beta_n < (n+\frac{1}{2})\pi$, figure 11 (*a*) shows that w_{0n} is positive, so these solutions are not physically possible. Of particular interest is the region $\beta_n < \frac{1}{2}\pi$, where the flow rate is higher than for the flow shown in figure 12. A solution exists in which the

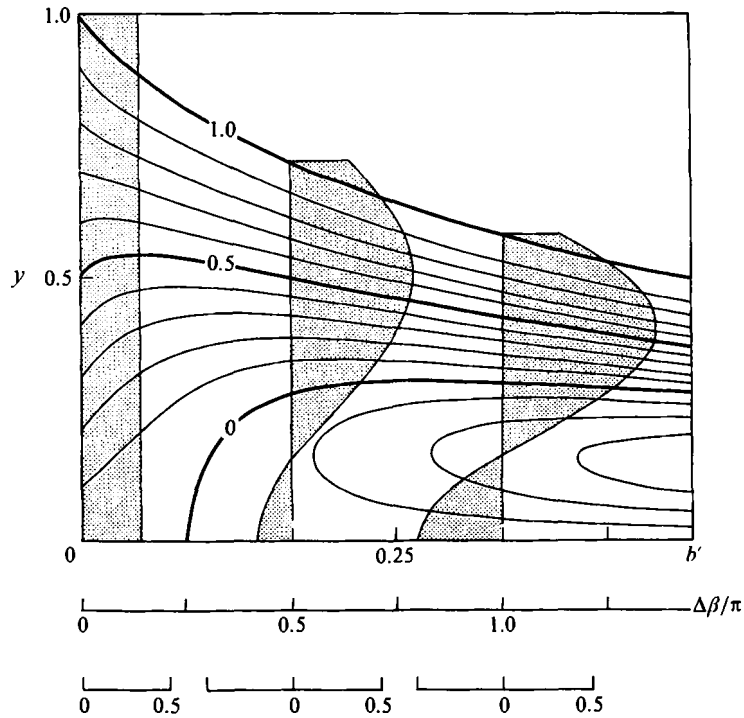

FIGURE 14. As figure 12 but for $\beta_n = \frac{3}{2}\pi$, $\beta_s = \frac{3}{2}\pi$.

enclosed self-similar flow simply passes through the narrowest section, accelerating as the channel converges and decelerating as the channel diverges, and a separation point occurs in the divergent section at the point at which the channel width has increased to $\beta = \beta_p = \frac{1}{2}\pi$. In this case, the flow is controlled not at the narrowest section but at the separation point, and downstream of this point the flow is exactly that shown in the divergent section of figure 12. Similar behaviour has been found for single-layer (Armi & Farmer 1986) and two-layer plunging flows (Williams & Armi 1991). These solutions must be viewed with caution since at the separation point, $db/dx \neq 0$ and so $dw/dz \to \infty$ and the assumptions of the model are violated.

Figure 11 (*a*) shows that there are ranges of $\beta_n > \pi$ where $w_{0n} \leqslant 0$, and solutions can be found for these ranges of β_n. The solutions all contain at least one region in which the density surfaces diverge downstream of the separation point and all reach a value of β in the divergent section where $dy/dz < 0$, and so the fluid is statically unstable in some part of the channel. The solution for $\beta_s = \beta_n = \frac{3}{2}\pi$ is shown in figure 14. In this solution, and in all others like it, the first downstream location at which $dy/dz < 0$ is quite close to the separation point. The presence of a region of statically unstable fluid suggests looking for solutions with more than one region of stagnant, constant-density fluid. The simplest flow of this type has symmetric stagnant regions at the top and bottom of the channel, and the flow is confined to a jet in the centre of the channel. It is also possible to find a flow with multiple jets, decoupled from each other by regions of stagnant fluid. As in the case of a single jet at the centre of the channel, a solution is found by stacking multiple vertically rescaled copies of the solution just described, inverting every other copy. This scenario leads to a flow with multiple jets, with intervening regions of stagnant fluid that all start at the same alongstream location.

3.2. *Comparison of experiments with theory for bifurcating flows*

For the flow shown in figure 7(*a*, *b*) velocity profiles at the narrowest section, and 10 cm downstream of the narrowest section, are shown in figure 8(*b*, *c*). The moving region at the narrowest section extends to the free surface, where there is a thin boundary layer; the lack of data points above 17 cm in figure 8(*b*) is due to a lack of clear particle streaks. Figure 8 also shows velocity profiles using the channel width parameter (20).

For this flow, at the narrowest section $\beta_n = 0.62\pi$ and the theory predicts the separation point to be somewhat upstream of the narrowest section. The fact that the separation point is further downstream and the moving region in the divergent section is thicker than predicted by theory can again be explained, as in §2, by considering the effect of growing sidewall boundary layers on both the effective channel width and the effective positions of the narrowest section. The observed vertical structure of the velocity profile in the divergent section is similar to that predicted by the theory.

The interface between the moving fluid and the theoretically stagnant region is unstable. This is seen in figure 7(*b*), a streak photograph of the region downstream of the narrowest section. At the bottom of the channel the supercritical jet can be seen, and above this, large eddies caused by instability of the interface between the jet and the overlying fluid are apparent. Above these eddies, the streak photograph and the vertical dye lines in figure 7(*a*) also show that there are considerable turbulent motions in the overlying fluid, but the mean velocity is slow, in agreement with the theory. In fact, the turbulence helped form this region of nearly stagnant fluid.

The upside-down version of the flow shown in figure 7(*a*) is seen in figure 9, a flow with the withdrawal slit at the top of the channel. This flow also has a transition from a structure-0 to structure-1 profile and the flow is again nearly uniform upstream of the narrowest section. In the divergent section of the channel, the flow separates from the base of the channel to match the downstream condition imposed by the withdrawal slit. The theoretical description of the flow is almost exactly an inverted version of the flow shown in figure 7, and using the Boussinesq approximation makes the symmetry of the theoretical description exact.

A more complex separating flow, shown in figure 15(*a*) (plate 4), was studied by withdrawing fluid from both the top and bottom of the channel at equal flow rates. The total volume flux was high enough that the flow coming from the reservoir was supercritical at the narrowest section with respect to the mode controlling structure 2 and was vertically uniform. In the divergent part of the channel, there is a transition to a structure-2 profile as the flow splits into two supercritical portions, separated by a region of stagnant, constant-density fluid which dynamically isolates the two moving regions. If the flow is considered to be Boussinesq, the two moving regions are each dynamically identical to the flows shown in figures 7 and 9.

A particle streak photograph of the flow in the divergent section of the channel, figure 15(*b*) (plate 4), dramatically illustrates the region of stagnant fluid. Velocity profiles of the flow, measured at the narrowest section and 10 cm upstream and downstream of the narrowest section, are shown in figure 16(*a–c*). At the narrowest section $\beta_n = 0.65\pi$. This figure also shows theoretical velocity profiles. The deviations from the theory are similar to those discussed earlier. Close to the separation point there is considerable curvature of the streamlines and just upstream of the separation we again observe vertical shear not predicted by the hydrostatic theory (figure 16*b*).

Just as there were two possible transitions from structure 0 to structure 1, there are also two possible transitions from structure 0 to structure 2. Figure 17 (plate 4), the

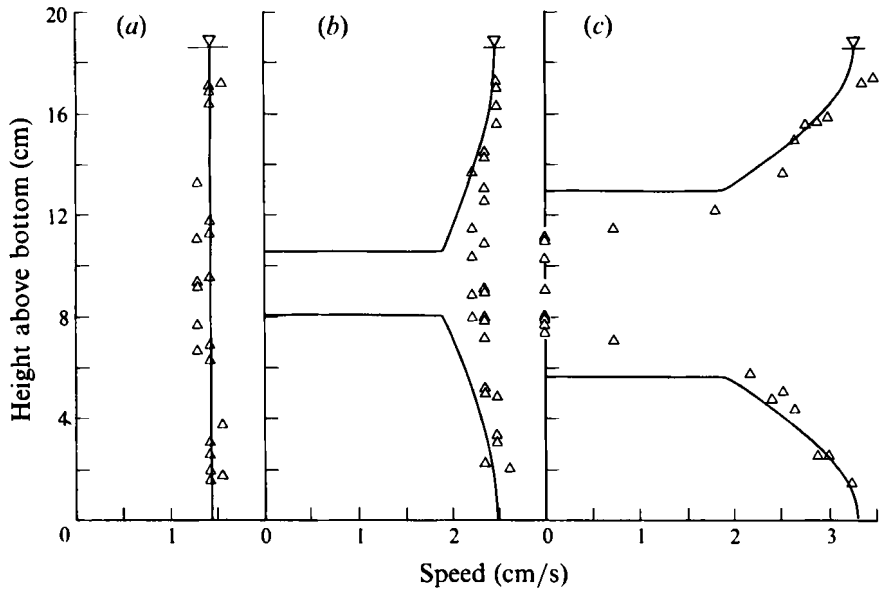

FIGURE 16. Velocity profiles of the enclosed self-similar flow with structure-2 separating flow in the divergent section shown in figure 15(*a*). (*a*) 10 cm upstream of the narrowest section, $b = 2.9$ cm, $b' = 1.45$, $\Delta\beta/\pi = 0.29$. (*b*) At the narrowest section, $b = 2.0$ cm, $b' = 1$, $\Delta\beta/\pi = 0$, $\beta_n = 0.65\pi$ (*c*) 10 cm downstream of the narrowest section, $b = 2.5$ cm, $b' = 1.25$, $\Delta\beta/\pi = 0.16$.

second flow of this type, was made by placing the withdrawal slit at the centre of the channel. The flow in the convergent section of the channel is vertically nearly uniform, and is identical to that shown in the other flows discussed in this section. In the divergent section, the flow accelerates as a supercritical structure-2 jet at mid-depth. Although not shown, flows with higher-order structure in the divergent section have been made by using more withdrawal slits.

4. Subcritical internal self-similar flows

For a particular reservoir stratification and flow rate, the range of density surfaces that flow through the contraction in the internal self-similar flow were shown in §2 to be determined by the control at the narrowest section. Here, we explore the result of breaking this constraint by arranging the downstream conditions to withdraw fluid from a greater range of densities than required by a controlled internal self-similar flow.

A series of experiments were performed with two downstream withdrawal slits with equal volume flux flowing into each slit. Figure 2(*a*) is a photograph of the experiment that shows the two withdrawal slits. The flow rates were low and the withdrawal points were located so that in all cases the moving fluid is bounded above and below by stagnant fluid rather than by the upper or lower boundaries. When there is only one withdrawal point, a structure-2 internal self-similar flow, similar to that shown in figure 5, occurs. A series of flows with the same total volume flux but increasing sink separations are shown in figure 18(*a–c*) (plate 5).

In figure 18(*a*), the withdrawal slots are 5 cm apart and the flow is similar to that shown in figure 5. The flow is still controlled at the narrowest section and has a structure-2 velocity profile in most of the channel. The downstream conditions cause a weak varicose-like internal hydraulic jump in the divergent section of the channel,

approximately 14 cm downstream of the narrowest section, to a subcritical flow that still has a structure-2 profile. This is characterized by a slight spreading of the isopycnals, while the vertical dye lines show the form of the velocity profile.

The effect of increasing the sink separation to approximately 7 cm is shown in figure 18(*b*). A larger view of this flow, showing the downstream sinks, is shown in figure 2(*a*). The internal hydraulic jump has propagated upstream through the control and the flow at the narrowest section is now subcritical with respect to the lowest mode, which controls structure 2. The range of moving isopycnals is now controlled by the downstream conditions. The vertical structure of the flow coming from the stagnant reservoir is still determined by the virtual controls in the convergent section and so, despite the lack of a control at the narrowest section, the flow coming from the stagnant reservoir is again an internal self-similar flow with vertical structure 2. Since the flow is subcritical with respect to structure 2, in the immediate vicinity of the narrowest section the flow is symmetric and thickens as the channel diverges, just as it thins as the channel converges. This symmetry makes the location of the effective narrowest section readily apparent; it is about 5 cm downstream of the geometric narrows. The symmetric behaviour does not continue far downstream. The flow at the narrowest section is supercritical with respect to the internal mode which controls structure 4 and, as the channel diverges, the flow slows and approaches the virtual control for that mode. As in the two-layer flow studied by Armi (1986), the flow remains supercritical with respect to the higher mode; here is splits into a flow with structure 4, having two internal jets as the channel diverges.

A flow with a sink separation of 9.5 cm is shown in figure 18 (*c*). With this larger sink separation, the flow divides into two jets that are separated by a region of stagnant fluid at all points in the channel. There are now two dynamically isolated structure-2 flows, each controlled at the narrowest section.

Similar behaviour was seen when the flow was bounded below by the bottom of the channel. Figure 19 (plate 6) shows a flow with one sink at the bottom of the channel and a second sink 7 cm above the bottom of the channel. The volume flux into each sink was equal. The behaviour is analogous to that shown in figure 18(*b*) except that the upstream velocity profile has structure 1 and the bifurcation in the divergent section is to a flow with structure 3.

A complex flow, involving bifurcations of both external and internal flows, is shown in figure 20 (plate 6). The total volume flux is such that there is an enclosed self-similar flow in the convergent section of the channel. The complex behaviour in the divergent section arises when the withdrawal slot is significantly off mid-depth. Here, it is 12 cm above the bottom of the channel, and the total depth is 18 cm. In the divergent section of the channel, close to the narrowest section, the flow looks like the simple separating flow shown in figure 9. Further downstream, as the channel diverges, a second region of stagnant fluid appears and there is a transition from a structure-1 to a structure-2 velocity profile. Since the structure-1 flow is supercritical downstream of the narrowest section, we propose that in order for the transition to a structure 2 flow to take place, the flow must first pass through a weak hydraulic jump to a subcritical structure-1 flow. Then, as the channel diverges, the subcritical structure-1 flow slows and deepens as it approaches the structure-2 virtual control. The flow separates from the upper boundary, flows beneath a second layer of stagnant fluid and continues downstream as a supercritical structure-2 flow.

4.1. *Bifurcations of the internal self-similar solution*

In order to consider the possibility of asymmetric solutions in the divergent section of the channel, we look for bifurcations of the internal self-similar solution. We restrict our attention to the linear density profile. The form of the self-similar solution suggests seeking solutions of the form

$$y = k(\lambda)\, z + \epsilon w. \tag{32}$$

This is substituted into (8*a*) and terms of $O(\epsilon)$ give

$$[(1-z^2)\, w']' + \left(\frac{k}{1-k}\right) w = 0. \tag{33}$$

This is Legendre's equation, and non-trivial solutions $w = P_m(z)$ exist only if $k/(1-k) = m(m+1)$. For flows with the moving fluid against the bottom of the channel, $w = 0$ at $z = 0$ and so $m = 2n-1$. This defines a series of values of k, and hence of channel width, at which a bifurcation of the solution is possible. Each of these points is a place at which the solution admits a stationary disturbance. The case $n = 1, k = \frac{2}{3}$ is the control at the narrowest section. The other eigenvalues are the virtual controls of the self-similar flow. Guided by the analogous results seen in the two-layer flows and in the separating flows discussed in §3, downstream of the bifurcation we expect the flow to split into multiple jets that are supercritical with respect to the mode that is critical at the bifurcation.

With a similar approach, Benjamin (1981) looked for solutions adjacent to the self-similar solution and found that the same set of eigenvalues, here identified as virtual control points, were points that prevented the existence of a solution with a slightly perturbed reservoir function. In a complementary result, we see that when the reservoir function is not perturbed, the virtual control points allow branching of the self-similar solution.

5. Discussion

The series of experiments and solutions discussed here show major aspects of the hydraulics of a continuously stratified fluid as it flows from a stagnant reservoir through a contraction. Of particular importance are the strong constraints on upstream conditions due to the presence of a sequence of virtual controls as the flow leaves the stagnant reservoir. The upstream flow is always self-similar, and complex downstream conditions can only lead to upstream conditions that are either a single self-similar flow or a set of decoupled self-similar flows separated by non-moving stratified regions. There are two forms of the self-similar flow. One, which occurs when fluid is withdrawn from a limited range of densities, has a strongly depth-dependent velocity profile and we refer to it as an internal self-similar flow. The other, which occurs when fluid is withdrawn from all levels in the reservoir, has a nearly uniform vertical velocity profile and we refer to it as an enclosed self-similar flow.

Another important feature of the flows shown here is the presence of regions of stagnant, constant-density fluid. The controlled internal self-similar flows, which are asymmetric about the narrowest section and are fully supercritical in the divergent portion of the channel, have these regions throughout the channel. We have also demonstrated both internal and external self-similar flows that are not controlled at the narrowest section. In these cases, the flow at the narrowest section is subcritical with respect to the lowest mode but is supercritical with respect to higher modes. Since the flow at the narrowest section is subcritical, it is symmetric about the narrowest section

and, as the channel diverges, the flow decelerates and approaches a virtual control with respect to a higher wave mode. Instead of passing through the virtual control and becoming subcritical with respect to that internal mode, the flow remains supercritical with respect to that mode and forms one or more fast-moving regions as the channel diverges. When this happens, separating isopycnals and regions of stagnant constant-density fluid always form in the divergent section of the channel.

Owing to the limited size of the experimental facility, most of the experiments shown here were conducted at low enough Reynolds numbers (approximately 500, based on the velocity and channel width at the narrowest section) that the flows were stable and mixing did not occur. Experiments conducted at higher flow rates (Reynolds number ≈ 1000) showed that flows whose large-scale structure is hydraulically controlled can give rise to unstable vertical velocity profiles with substantial turbulence and mixing in parts of the channel. In large-scale engineering and geophysical applications, we expect significant mixing in the supercritical regions of hydraulically controlled stratified flows. The hydraulic theory is useful in showing where this mixing is likely to occur.

The agreement between experiment and theory was always globally excellent. The theory predicts well the observed self-similar velocity distributions and the large-scale displacements and patterns of the density surfaces. The effect of sidewall boundary layers, neglected in the theory, is equivalent to considering a channel with sidewalls slightly narrower at each location and with the narrowest section displaced slightly downstream, typically about 5 cm for our experiments.

Our research is supported by the National Science Foundation. These experiments were begun by L. A. while on sabbatical at the Centre for Water Research, University of Western Australia, Perth, with support from the Australian Research Grants Scheme and a Gledden Visiting Senior Fellowship. Thanks to Professor J. Imberger and his colleagues in Perth for many thought-provoking discussions, as well as their hospitality.

REFERENCES

ARMI, L. 1986 The hydraulics of two flowing layers with different densities. *J. Fluid Mech.* **163**, 27–58.

ARMI, L. & FARMER, D. M. 1986 Maximal two-layer exchange through a contraction with barotropic net flow. *J. Fluid Mech.* **164**, 27–51.

BAINES, P. G. & GUEST, F. 1988 The nature of upstream blocking in uniformly stratified flow over long obstacles. *J. Fluid Mech.* **188**, 23–45.

BENJAMIN, T. B. 1981 Steady flows drawn from a stably stratified reservoir. *J. Fluid Mech.* **106**, 245–260.

BERNSTEIN, A., HEISER, W. H. & HEVENOR, C. 1967 Compound-compressible nozzle flow. *Trans. ASME* E: *J. Appl. Mech.* **34**, 548–554.

LONG, R. R. 1953 Some aspects of the flow of stratified fluids. I. A theoretical investigation. *Tellus* **5**, 42–58.

LONG, R. R. 1953 Some aspects of the flow of stratified fluids. III. Continuous density gradients. *Tellus* **7**, 341–357.

SMITH, R. B. 1985 On severe downslope winds. *J. Atmos. Sci.* **42**, 2597–2603.

WILLIAMS, R. & ARMI, L. 1991 Two-layer hydraulics with comparable internal wave speeds. *J. Fluid Mech.* **230**, 667–691.

WOOD, I. R. 1968 Selective withdrawal from a stably stratified fluid. *J. Fluid Mech.* **32**, 209–223.

YIH, C.-S. 1969 A class of solutions for steady stratified flows. *J. Fluid Mech.* **36**, 75–85.